ACS OMEGA

http://pubs.acs.org/journal/acsodf

Article

Synthesis and Application of $AgBiS_2$ and Ag_2S Nanoinks for the Production of IR Photodetectors

Tatsuya Nakazawa, Donghyun Kim, Yusuke Oshima, Hiroki Sato, Jusang Park,* and Hyungjun Kim*

Cite This: *ACS Omega* 2021, 6, 20710−20718

Read Online

ACCESS | Metrics & More | Article Recommendations | Supporting Information

ABSTRACT: Nanoinks composed of quantum dots (QDs) are applied in light-receiving devices and light-emitting devices such as solar cells and displays. However, since the most widely used QDs, PbS and CdS, are toxic and environmentally concerning, alternative materials need to be developed. We synthesized and analyzed Ag chalcogenide nanoparticles, including $AgBiS_2$ and Ag_2S nanoparticles, which are eco-friendly materials. $AgBiS_2$ and Ag_2S QD films were prepared by spin-coating nanoparticle solutions and subsequent heat treatment. The effects of the heat treatment on residual ligands and photoluminescence were determined by surface analysis. The photocurrent response of the $AgBiS_2$ and Ag_2S QD films was measured in the near-infrared region, and the effect of the heat treatment temperature was investigated. The results indicate that $AgBiS_2$ and Ag_2S are prospective materials for near-infrared photodetectors.

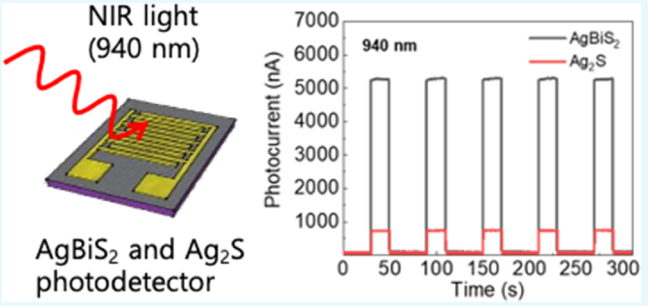

INTRODUCTION

In recent years, the semiconductor industry has shown great interest in printed electronics, which do not require significant capital investment.[1] Among the available printing technologies, those using nanoinks, which can provide fine patterning and functionality, have been attracting attention.[2,3] After printing, the nanoinks are sintered to improve the crystallinity of ink nanoparticles. The size of the nanoparticles in nanoinks is usually 10−100 nm, so sintering can be carried out at low temperatures.[4,5] Thus, films and circuits can be formed on heat-sensitive substrates such as polymers, and nanoinks are expected to be applied in wearable devices, bendable devices, and biosensors.[6−8]

On the other hand, the nanoparticles in nanoinks are covered with protective organic layers that prevent aggregation. These layers and ligands have been shown to affect electrical properties. Therefore, it is important to investigate the effects of residual organic substances as functional groups derived from protective layers and exchanged ligands bound to nanoparticle surfaces.[9] For example, the functional groups on the surface of nanoparticles have been shown to result in electrical disequilibrium and affect semiconductor properties, such as photoluminescence (PL) and UV−vis absorption.[10−12] Generally, heat treatment (postannealing) after nanoink coating can eliminate the effects of the functional groups present in the protective layer. Postannealing is used not only to remove the protective layer and ligands but also to obtain optimal optical properties via grain growth or enhanced crystallinity.[13−15] The postannealing temperature and time are important because agglomeration and sintering proceed more easily at lower temperatures in nanoparticles than in bulk specimens.[16] Therefore, tailoring surface ligands and preventing thermal agglomeration with appropriate heat treatment conditions are necessary to produce beneficial properties.[17,18]

Quantum dot (QD) nanoparticles have been used in lighting, displays, and various sensors to improve device performance. Semiconductor QD nanoparticles, such as PbS and CdS, are commonly used at present. However, PbS and CdS QDs have a high environmental load and are affected by restriction of hazardous substances (RoHS) directives, so QD nanoparticles that do not contain harmful heavy metals are highly desired.[19−21] Recently, Ag-based materials such as $AgBiS_2$ and Ag_2S nanoparticles have attracted a great deal of attention since they can be easily synthesized and exhibit sufficient characteristics in solar cell applications. In particular, they are promising materials for near-infrared photodetectors that are used at room temperature in many technologies, such as light detection and ranging (LIDAR), medical imaging devices, and smartphone components due to their band gap.[9,22−25] Moreover, they are compliant with RoHS directives.[9,24−28] However, studies of Ag_2S and $AgBiS_2$ have mainly focused on nanoparticle synthesis and a few have been carried out to elucidate the effect of the heat treatment process, which is essential for device fabrication.[9,29−33] Organic

Received: July 2, 2021
Accepted: July 23, 2021
Published: August 2, 2021

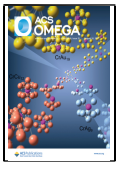

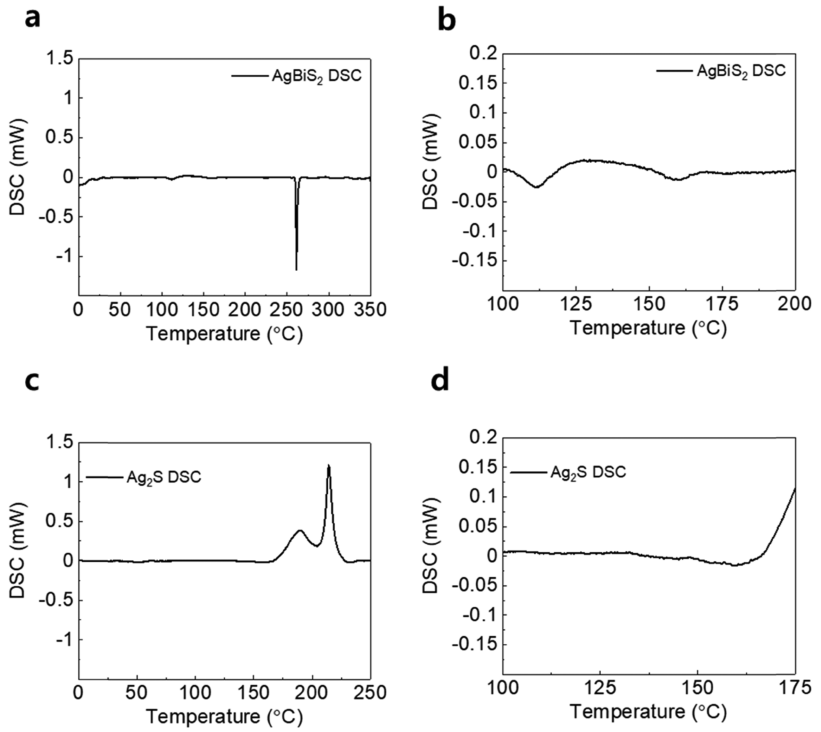

Figure 1. DSC curves for (a) $AgBiS_2$, (b) $AgBiS_2$ from 100 to 200 °C, (c) Ag_2S, and (d) Ag_2S from 100 to 175 °C.

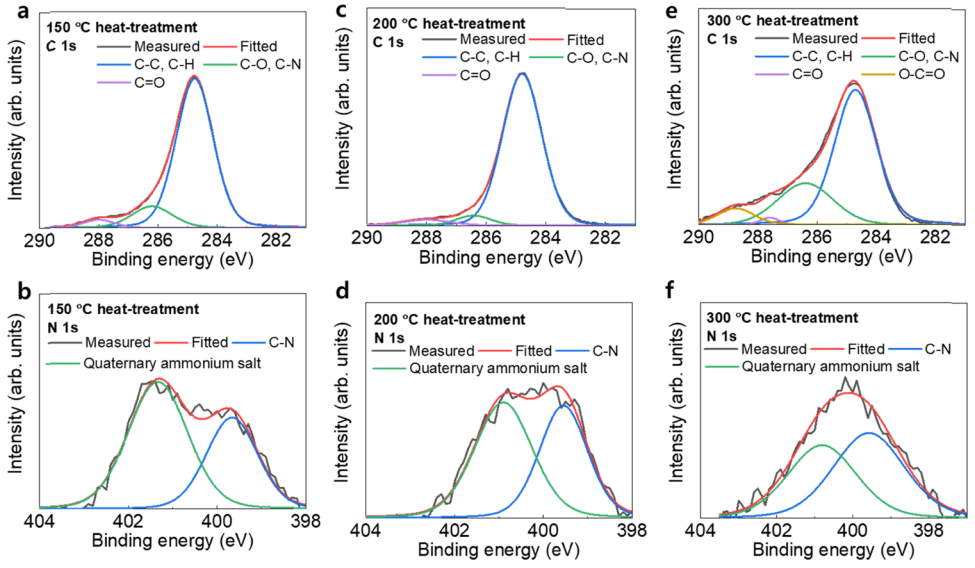

Figure 2. XPS spectra of $AgBiS_2$ heat-treated at 150 °C: (a) C 1s and (b) N 1s spectra. XPS spectra of $AgBiS_2$ heat-treated at 200 °C: (c) C 1s and (d) N 1s spectra. XPS spectra of $AgBiS_2$ heat-treated at 300 °C: (e) C 1s and (f) N 1s spectra.

substances used as protective layers and dispersants for nanoparticles interfere with charge localization, resulting in the formation of defects and quantum confinement effects on nanoparticle surfaces.[34−38] Postannealing is conducted after coating with nanoinks to remove organic substances. Therefore, clarifying the relationship between the postannealing temperature and the organic substances on nanoparticle surfaces is essential for improving the performance of photodetection devices. In this study, we synthesized $AgBiS_2$ and Ag_2S thin films by spin-coating using chemically synthesized nanoinks. The effect of surface ligands on the annealing temperature was determined by chemical analysis and PL measurements. Then, we elucidated the relationship between organic substances on the nanoparticle surfaces and the postannealing temperature. Additionally, we investigated the effect of heat treatment temperature on the photocurrent response.

RESULTS AND DISCUSSION

$AgBiS_2$ and Ag_2S nanoinks were synthesized in TANAKA KIKINZOKU KOGYO K.K. Tokyo, Japan. The average particle size of the synthesized $AgBiS_2$ was 8.75 nm, and that of Ag_2S was 14.86 nm (Figure S1). Since the concentration of the nanoink is 20 mg/mL in both samples, the viscosity of the nanoink is almost equal to that of the solvent toluene (554.2 ± 3.3 μPas).[39] Uniform $AgBiS_2$ and Ag_2S films were prepared by

https://doi.org/10.1021/acsomega.1c03463
ACS Omega 2021, 6, 20710−20718

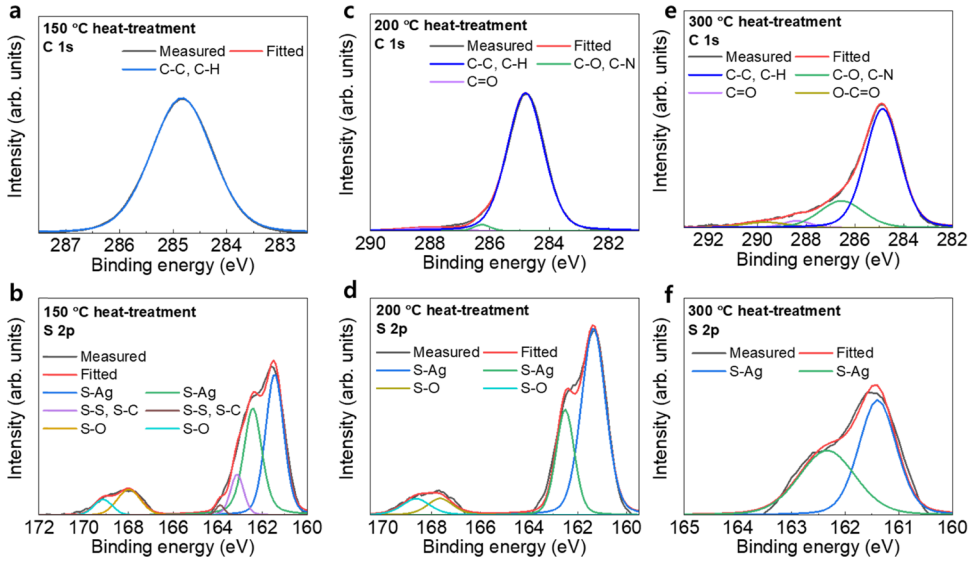

Figure 3. XPS spectra of Ag_2S heat-treated at 150 °C: (a) C 1s and (b) S 2p spectra. XPS spectra of Ag_2S heat-treated at 200 °C: (c) C 1s and (d) S 2p spectra. XPS spectra of Ag_2S heat-treated at 300 °C: (e) C 1s and (f) S 2p spectra.

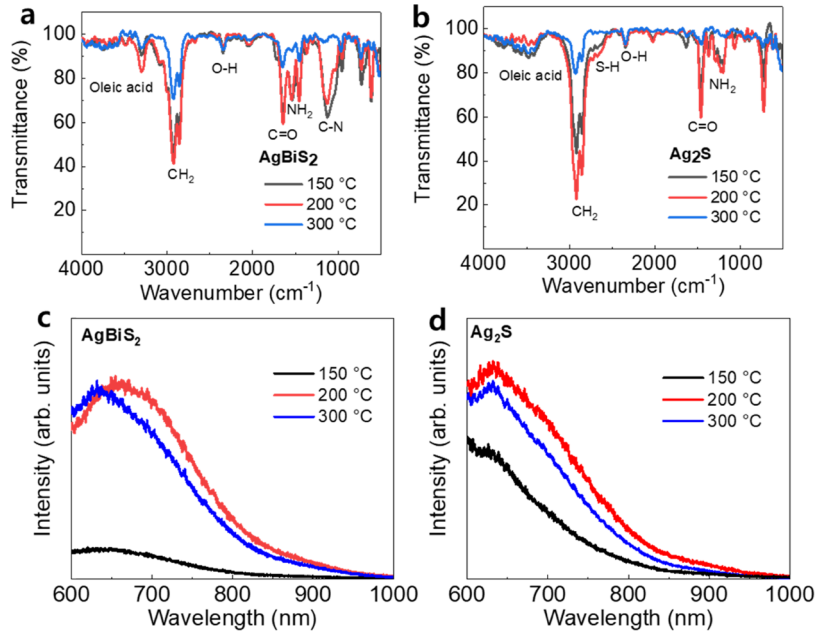

Figure 4. FT-IR spectra of (a) $AgBiS_2$ and (b) Ag_2S. PL spectra of (c) $AgBiS_2$ and (d) Ag_2S.

spin-coating on SiO_2/Si substrates. Then, the samples were heat-treated at 150−300 °C to remove solvents and ligands. Differential scanning calorimetry (DSC) was conducted to determine the volatility or decomposition temperature of the solvents and ligands in the nanoinks. The DSC results confirmed that most of the solvents and ligands in both of the nanoinks were removed at 160−170 °C (Figure 1). The peaks observed below 100 °C and at approximately 100 °C represent the volatilization of solvents and the evaporation of water, respectively. The peak at 220 °C for Ag_2S is attributed to the pyrolysis of thiourea.[40] Furthermore, the peak at 255 °C for $AgBiS_2$ shows a triple eutectic point, and the peak at 178 °C for Ag_2S represents the α-to-β phase transition.[41,42] However, ligands remain coordinated to the nanoparticle surfaces. Therefore, X-ray photoelectron spectroscopy (XPS) analysis was carried out to investigate the remaining surface ligands.

For $AgBiS_2$, the C and N atoms of amines were investigated. The chemical states of C and N were estimated from the binding energies observed in narrow XPS scans (Figure 2).[43] The C−C/C−H peak at 284 eV exhibited the highest intensity, followed by the C−O/C−N peak at 286 eV and the C═O peak at 287 eV. In addition, a O−C═O peak was detected at 289.0 eV in the film heat-treated at 300 °C. O−C═O bonds were generated by oleic acid changing from monodentate to bidentate.[44] In the N spectra, two peaks attributed to C−N and a quaternary ammonium salt were observed at 399 and 401 eV, respectively. Additionally, the intensity of the peak associated with the quaternary ammonium salt decreased with increasing heat treatment temperature. Many quaternary ammonium salts are pyrolyzed

https://doi.org/10.1021/acsomega.1c03463
ACS Omega 2021, 6, 20710−20718

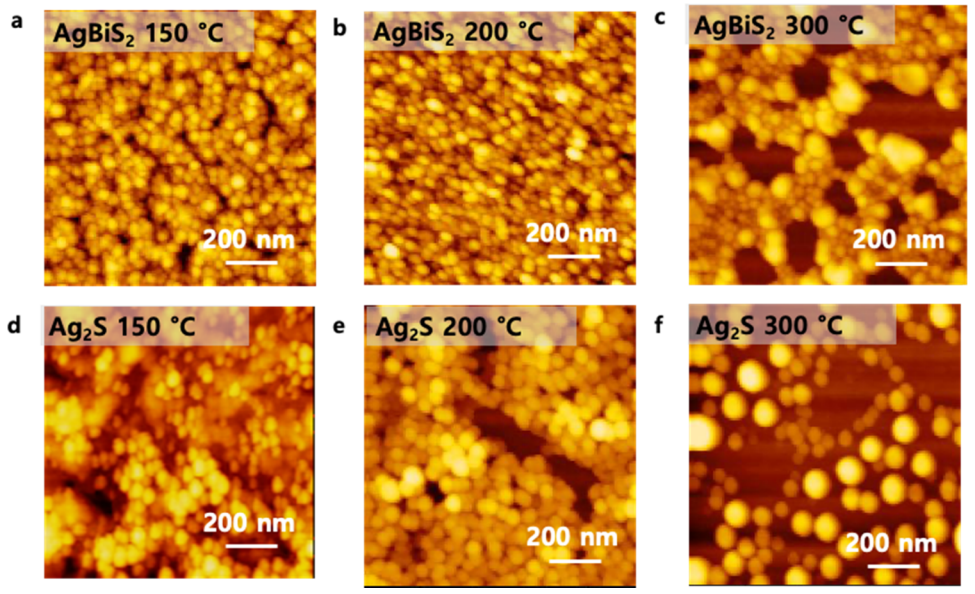

Figure 5. AFM images of $AgBiS_2$ heat-treated at (a) 150 °C, (b) 200 °C, and (c) 300 °C. Surface AFM images of Ag_2S heat-treated at (d) 150 °C, (e) 200 °C, and (f) 300 °C.

at approximately 200 °C; the intensity of the peak associated with the quaternary ammonium salt decreased after the film was heat-treated above 200 °C because the quaternary ammonium salt thermally decomposed.[45]

For Ag_2S, C peaks and S peaks (attributed to thiol) were investigated (Figure 3). First, the carbon spectrum of the sample heat-treated at 150 °C shows that only a peak associated with C−C or C−H bonds is detected (284 eV). This is attributed to dodecanethiol, which was used as a ligand, remaining on the surface in large quantities. The vapor pressure of dodecanethiol increased with increasing temperature, but it did not sufficiently volatilize at 150 °C.[46] As the temperature increased, the observed behavior was similar to that of $AgBiS_2$, and a bidentate O−C═O peak at 289.0 eV was observed after heat treatment at 300 °C. The chemical states of sulfur associated with the thiol group were also analyzed. The sample heat-treated at 150 °C displays peaks attributed to S−Ag, S−S, S−C, and S−O bonding. The Ag−S, S−S, S−C, and S−O peaks were clearly identified as belonging to Ag_2S, elemental sulfur, thiol, and sulfur oxides (SO_x) produced during the heat treatment, respectively. The peaks at 162.5 eV ($2p_{1/2}$) and 161.3 eV ($2p_{3/2}$) were attributed to Ag−S.[47] The peaks at 163.7 eV ($2p_{1/2}$) and 162.6 eV ($2p_{3/2}$) were derived from S and S−C, respectively.[43,48] SO_x peaks were also observed at 168.7 eV ($2p_{1/2}$) and 167.7 eV ($2p_{3/2}$).[43] Upon heating to 200 °C, the S−S and C−S peaks disappeared due to the evaporation of elemental sulfur and sufficient volatilization of dodecanethiol.[49] In the sample heat-treated at 300 °C, the S−O peak disappeared, and sulfur oxide that formed during the heat treatment was removed.

Fourier transform infrared (FT-IR) spectroscopy was performed to investigate the functional groups (Figure 4a,b). The FT-IR spectrum of $AgBiS_2$ exhibited the characteristic modes of oleyl groups. Asymmetric and symmetric CH_2 stretching modes were observed at 2926 and 2856 cm^{-1}, respectively.[50] In addition, the broad peaks at 3100−3200 cm^{-1} were assigned to the dimers of oleic acid.[51] The C═O stretching mode observed at 1647 cm^{-1} was assigned to carboxylic acid, and the O−H stretching mode observed at 2665 cm^{-1} was assigned to dimeric COOH.[52] A peak derived from oleyl amine was seen in the FT-IR spectra of both $AgBiS_2$ and Ag_2S. The peak at 1544 cm^{-1} was associated with NH_2 scissoring, and the peak at 3302 cm^{-1} was attributed to N−H stretching.[53] The peak located at 1637 cm^{-1} was assigned to N−H rocking vibrations in organic amines, and the broad peaks located at 700−900 cm^{-1} were due to N−H vibrations.[54] Additionally, a C−N stretching mode peak was observed at 1118 cm^{-1}.[55] Peaks derived from dodecanethiol were also detected in the FT-IR spectrum of Ag_2S. The broad peaks at 2500−2600 cm^{-1} were due to S-H stretching vibrations. The FT-IR results indicated that the samples heat-treated at 300 °C had lower-intensity N (oleyl amine) or S (dodecanethiol) peaks. Quaternary ammonium salts and oleic acid dimers were present due to an excess of amines and oleic acid, which were used as protectants during synthesis. The excess protectants were removed by centrifugation, but those that could not be removed entirely were detected as quaternary ammonium salt or oleic acid dimer-free ligands. Based on the above chemical analysis, it was determined that not only the types of ligands on the nanoparticle surfaces but also their binding and coordination states changed with increasing annealing temperature. The PL spectra of $AgBiS_2$ and Ag_2S heat-treated at 200 °C exhibited the highest intensity (Figure 4c,d). The enhanced PL between 150 and 200 °C was attributed to the effects of the ligands on the surface of the QDs.[56] For the 150 °C heat treatment, the surface of the QDs was not passivated due to the effects of excess ligands. The excess ligands contained amine or thiol groups, resulting in surface defects and weakened electrical properties.[35−37] The DSC results suggested that the excess ligands, which weakened the electrical properties, volatilized upon heat treatment at 200 °C; however, the ligands remained on the surface. Moreover, the PL intensity was reduced after heat treatment at 300 °C, which was sufficient to remove the ligands. A further analysis of the particles on the substrate was carried out to investigate the underlying cause for the decrease in PL intensity.

According to atomic force microscopy (AFM) observations, the particle sizes of the samples heat-treated at 150 and 200 °C

https://doi.org/10.1021/acsomega.1c03463
ACS Omega 2021, 6, 20710−20718

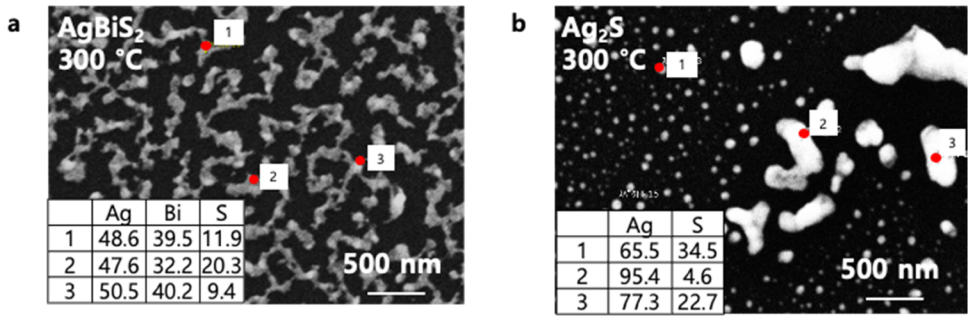

	Ag	Bi	S
1	48.6	39.5	11.9
2	47.6	32.2	20.3
3	50.5	40.2	9.4

	Ag	S
1	65.5	34.5
2	95.4	4.6
3	77.3	22.7

Figure 6. EDX point analysis of (a) $AgBiS_2$ and (b) Ag_2S heat-treated at 300 °C.

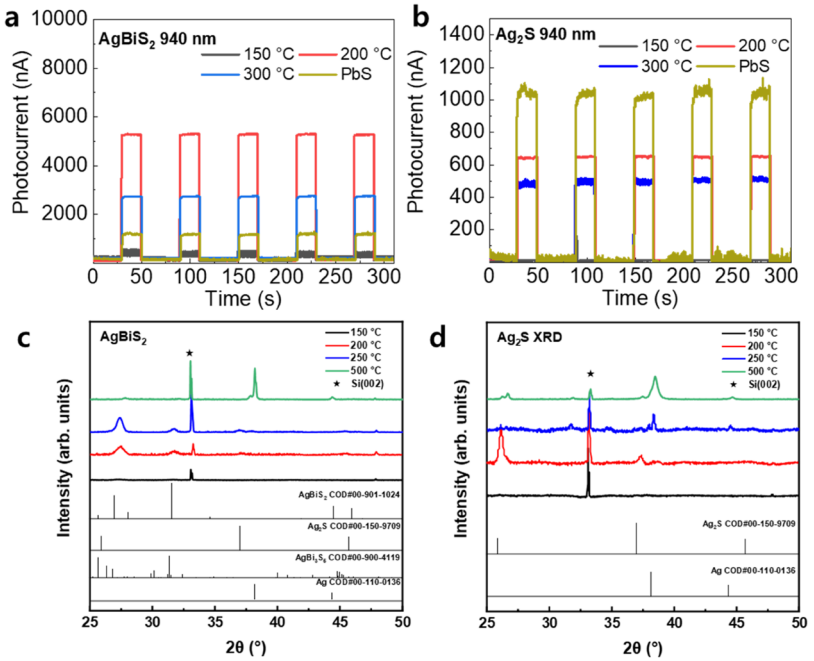

Figure 7. Photocurrent response (at 940 nm) of (a) $AgBiS_2$ and PbS and (b) Ag_2S and PbS. XRD pattern of (c) $AgBiS_2$ and (d) Ag_2S.

were nearly identical to the particle sizes of the pristine nanoinks, but heat treatment at 300 °C resulted in agglomeration (Figure 5). It has been reported that Ag_2S particles grow due to collective recrystallization above the phase-transition temperature (178 °C); accordingly, the Ag_2S film changes and exhibits an island-like surface morphology with increasing temperature.[41,57] Since the Ag−Bi−S system has a triple eutectic point from 250 to 260 °C, heat treatment at 300 °C impairs the thermal stability of the β-$AgBiS_2$ phase and causes phase segregation.[42] The composition of the particles was measured by energy-dispersive X-ray spectroscopy (EDX) point analysis. This analysis shows that phase segregation occurs in $AgBiS_2$ (Figure 6a). Likewise, EDX analysis of Ag_2S shows the presence of particles with a Ag-rich phase (Figure 6b). Ag precipitates when Ag_2S is heated in the presence of oxygen.[57] In this study, although heat treatment was performed under nitrogen gas flow, a small amount of oxygen in the reaction environment reacted with Ag_2S, resulting in Ag precipitation.

Photodetectors were fabricated by the thermal evaporation of Au/Ti (40/5 nm) electrodes on the $AgBiS_2$ and Ag_2S films. The photocurrent response of $AgBiS_2$ and Ag_2S was measured using 740, 850, and 940 nm pulsed light-emitting diode (LED) light. We also fabricated PbS devices for comparison, since PbS is the most widely used product in this field and one of the benchmark products in our research. A PbS film was made with a PbS QD ink (Sigma-Aldrich 900733) under the same coating conditions. The PbS film was heat-treated at 150 °C to prevent PL peak shifts (Figure S2e). The photocurrent and photocurrent response were monitored for all of the films. Both the $AgBiS_2$ and Ag_2S films heat-treated at 150 °C exhibited the lowest photocurrent response at each wavelength (Figures 7 and S2). The 10−90% response time of all samples was less than 0.8 s of the multimeter's time resolution. The highest photocurrent response for both samples (at each wavelength) was observed after annealing at 200 °C. $AgBiS_2$ heat-treated at 200 °C showed an approximately 5-fold higher photocurrent response than PbS. Ag_2S heat-treated at 200 °C was also shown to exhibit acceptable performance as an alternative material. The photocurrent response corresponds to the intensity of the PL signal, and the decrease in the photocurrent response of the 300 °C heat-treated samples is due to phase segregation and grain growth effects. The photocurrent response of $AgBiS_2$ and Ag_2S heat-treated at 500 °C was measured to further investigate the effect of phase segregation and grain growth. The photocurrent response of the $AgBiS_2$ film heat-treated at 500 °C was significantly lower than the photocurrent response of $AgBiS_2$ heat-treated at 200

https://doi.org/10.1021/acsomega.1c03463
ACS Omega 2021, 6, 20710−20718

°C. For Ag_2S, essentially no photocurrent response was observed. It was also found that the PL intensity decreased after heat treatment at 500 °C. Field emission scanning electron microscopy (FE-SEM) images indicated that particle agglomeration occurred, and coarse particles were obviously formed (Figures S3 and S4). The particles grew due to necking and sintering during heat treatment. Generally, the starting temperature for particle necking in coarse powders is considered to be approximately 0.6−0.8 the melting temperature.[58] It is also well known that the melting temperature of nanoparticles is lower than that of bulk specimens. The melting temperature of $AgBiS_2$ is 801 ± 4 °C, so 500 °C is sufficient for necking to initiate.[59] Therefore, one reason for the decrease in photocurrent response is that heat treatment at excessively high temperatures, such as 500 °C, causes grain growth and weakens the quantum confinement effect.[34] Furthermore, the EDX results for samples heat-treated at 500 °C indicate that phase segregation further occurred. As described above, Ag precipitates from Ag_2S after heat treatment in the presence of oxygen. Thus, for $AgBiS_2$, the precipitation of the Ag-rich phase suggests that Ag_2S was formed during phase segregation. On the other hand, since Ag_2S is the only stable compound in the Ag−S system, no phase segregation as in $AgBiS_2$ occurs.[41] The photocurrent of Ag_2S decreased due to the progress of grain growth with the increase of heat treatment temperature and the precipitation of Ag by the reaction of Ag_2S and oxygen at 500 °C. X-ray diffraction (XRD) analysis was performed on each sample to confirm the phase separation. Peak identifications for the XRD patterns were conducted using the Crystallography Open Database (COD) and QualX software program.[60−68] The multiple diffraction peak of Si substrate (002) was observed at around 33° from all samples.[69] Both $AgBiS_2$ and Ag_2S heat-treated at 150 °C had poor crystallinity, and no clear crystal peaks were observed. The reference peaks of $AgBiS_2$, Ag_2S, $AgBi_3S_5$, and Ag from the COD database are numbers of 00-901-1024 ($AgBiS_2$), 00-150-9709 (Ag_2S), 00-900-4119 ($AgBi_3S_5$), and 00-110-0136 (Ag), respectively.[70−73] For $AgBiS_2$ samples, $AgBiS_2$ peaks are observed in the heat-treated samples at 200 and 250 °C. On the other hand, the Ag_2S peak was observed around 37° slightly in the sample heat-treated at 250 °C. The main peak position of $AgBi_3S_5$ formed by phase segregation is almost the same as that of $AgBiS_2$, so it is not possible to separate the peaks clearly. In the heat-treated sample at 500 °C, the Ag peak was the main peak in the XRD pattern, indicating the progression of phase segregation and the formation of Ag_2S during the heat treatment at 500 °C. For Ag_2S samples, the Ag_2S peaks were observed in the sample heat-treated at 200 °C, but it was not clearly identified from the samples heat-treated at 250 and 500 °C. The Ag peaks resulting from the decomposition of Ag_2S were observed around 38 and 44° in the 250 and 500 °C heat-treated samples, respectively. Therefore, heat treatment at excessive temperatures causes phase segregation of $AgBiS_2$ and Ag_2S, leading to a decrease in the photocurrent response.

CONCLUSIONS

In this study, synthesized $AgBiS_2$ and Ag_2S nanoinks were spin-coated onto Si/SiO_2 substrates and heat-treated. Increasing the heat treatment temperature reduced the amount of surface functional groups, including N (amine) and S (thiol) groups, and defects on the particle surface were diminished. However, heat treatment at 300 °C reduced the PL strength, even though ligands were sufficiently removed. $AgBiS_2$ and Ag_2S photodetectors were prepared to measure the photocurrent response by depositing comb-shaped electrodes. The photocurrent response to near-infrared light was measured, and both $AgBiS_2$ and Ag_2S generated the highest photocurrent response after being heat-treated at 200 °C. Heat treatment removed excess protectants and ligands in the nanoinks, which improved the photocurrent response of $AgBiS_2$ and Ag_2S. Heat treatment above the phase-transition temperature ($AgBiS_2$: 255 °C, Ag_2S: 178 °C) caused phase segregation, and the stoichiometry of the materials deviated. In addition, the photocurrent response of $AgBiS_2$ was 5-fold higher than that of PbS particles prepared from a commercial PbS nanoink. $AgBiS_2$ and Ag_2S are eco-friendly and exhibit promising potential as photodetection materials due to their simple fabrication by spin-coating and their high photocurrent response in the near-infrared region. Additionally, $AgBiS_2$ and Ag_2S should be heat-treated below the phase-transition temperature to remove excess ligands.

EXPERIMENTAL DETAILS

Materials Used to Prepare the $AgBiS_2$ and Ag_2S Nanoinks. Silver acetate (Ag(OAc)) was synthesized at TANAKA Kikinzoku Kogyo K.K. (TANAKA) from silver(I) nitrate ($AgNO_3$), which was provided by TANAKA, using an anion exchange reaction. Bismuth(III) acetate ($Bi(OAc)_3$) was supplied by Sigma-Aldrich. Oleic acid, oleyl amine, and dodecanethiol were supplied by Tokyo Chemical, Inc. Sulfur, acetone, toluene, and methanol were supplied by Kanto Chemical. All products were used without further purification.

Preparation and Characterization of the $AgBiS_2$ and Ag_2S Nanoinks. $AgBiS_2$ and Ag_2S nanoinks were synthesized as described in a previous paper with slight modification.[9,74] To prepare $AgBiS_2$, 0.8 mmol of Ag(OAc) and 1.0 mmol of $Bi(OAc)_3$ were mixed in 5.5 mL of oleic acid contained in a necked flask. The mixture was degassed, and the flask was filled with N_2. Then, the mixture was stirred at 100 °C for 1 h. Sulfur (1.0 mmol) in 5 mL of oleyl amine was added to the solution, and the mixture was stirred for 5 min. After cooling to room temperature, $AgBiS_2$ nanoparticles were isolated by adding acetone and purified by centrifugation. After removing the solution, the nanoparticles were dispersed in toluene, isolated with acetone, and then purified by centrifugation. The process was repeated two times. Finally, the nanoparticles were dispersed in toluene.

To prepare Ag_2S, 0.8 mmol of Ag(OAc) and 0.4 mmol of thiourea were added to oleyl amine/dodecanethiol (59/1). The mixture was degassed, and the reaction container was filled with N_2. Then, the mixture was stirred at 200 °C for 5 min. After cooling to room temperature, Ag_2S nanoparticles were isolated by adding a small amount of methanol and purified by centrifugation. After removing the solution, the nanoparticles were dispersed in toluene, isolated with ethanol, and then purified by centrifugation. The process was repeated two times. Finally, the nanoparticles were dispersed in toluene. The nanoink particles were observed by transmission electron microscopy (TEM) (JEOL Ltd., JSM-1400F). ImageJ was used to measure particle size distributions.[75−77]

Preparation and Characterization of the Films. $AgBiS_2$ and Ag_2S films were fabricated on clean Si/SiO_2 substrates by spin-coating (Japan create, MSC-200D). The spin coater was operated at 2000 rpm for 30 s. The films were spin-coated three times layer by layer. The coated films were heat-treated

https://doi.org/10.1021/acsomega.1c03463
ACS Omega 2021, 6, 20710−20718

at 150−300 °C to remove organic solvents and ligands under a 50 sccm N_2 flow. A PbS QD ink was purchased from Sigma-Aldrich (No. 900733) for comparison and spin-coated in the same way at 2000 rpm for 30 s; the resulting film was heat-treated at 150 °C under a 50 sccm N_2 flow.

Surface morphologies were analyzed by AFM (Hitachi High-Tech Corporation, Nanocute). Surface images were obtained by FE-SEM (JEOL Ltd., JSM-7610F-Plus). PL was monitored using a LabRAM ARAMIS (HORIBA, Ltd., 532-nm-wavelength laser). Chemical states were determined by XPS (Thermo Fisher Scientific, Inc., K-Alpha X-ray Photoelectron Spectrometer System). Organic functional groups were analyzed by FT-IR (Shimadzu Corporation, IRPrestage-21). Chemical composition analysis was performed with SEM (JEOL Ltd., JSM-7800F Prime) and EDX (Oxford Instruments plc, Xmax Extreme). XRD patterns were measured using Ultima IV (Rigaku Corporation, Cu Kα). The crystal structure was identified by comparing the XRD pattern with a reference in the COD database and the calculated pattern. The used COD data numbers were 00-901-1024 ($AgBiS_2$), 00-150-9709 (Ag_2S), 00-900-4119 ($AgBi_3S_5$), and 00-110-0136 (Ag), respectively.[70−73]

Fabrication of Photodetectors. Photodetector electrodes were deposited by a thermal evaporator (SNTEK Co., Ltd., MEP5004) with a comb-like shadow mask on the $AgBiS_2$ and Ag_2S films. Au/Ti (40/5 nm) was deposited, with Au acting as the electrode and Ti acting as the adhesion layer.

IR Response Measurements. W LEDs were used as the light source for photocurrent response measurements. Three LED lights were mounted on a universal board. The universal board was programmed to function with the pulsed light on for 5 s and the pulsed light off for 10 s. The photocurrent response was measured using a voltage/current meter (Keithley 2400, Tektronix, Inc. Keithley Instruments) with a bias voltage of 0.5 V. The device was connected with alligator clips, and pressed indium grains were used as contacts.

■ ASSOCIATED CONTENT

Supporting Information

The Supporting Information is available free of charge at https://pubs.acs.org/doi/10.1021/acsomega.1c03463.

> Photo and TEM image of the $AgBiS_2$ and Ag_2S nanoink; particle size distribution in the nanoinks, as calculated by image analysis; photocurrent response of $AgBiS_2$ and PbS at 740 and 850 nm; photocurrent response of Ag_2S and PbS at 740 and 850 nm; PL spectra of PbS; photocurrent response of $AgBiS_2$ and Ag_2S heat-treated at 500 °C; PL spectra of $AgBiS_2$ and Ag_2S heat-treated at 200 and 500 °C; and surface morphology and EDX point analysis of $AgBiS_2$ and Ag_2S heat-treated at 500 °C (PDF)

■ AUTHOR INFORMATION

Corresponding Authors

Jusang Park − *School of Electrical and Electronic Engineering, Yonsei University, Seoul 03722, Republic of Korea;* Present Address: Advanced Institute of Convergence Technology, 145 Gwanggyo-ro, Yeongtong-gu, Suwon-si, Gyeonggi-do 16229, Republic of Korea; Email: jusang@yonsei.ac.kr

Hyungjun Kim − *School of Electrical and Electronic Engineering, Yonsei University, Seoul 03722, Republic of Korea;* orcid.org/0000-0003-2256-8046; Email: hyungjun@yonsei.ac.kr

Authors

Tatsuya Nakazawa − *School of Electrical and Electronic Engineering, Yonsei University, Seoul 03722, Republic of Korea; Metallic Materials Development Department, TANAKA KIKINZOKU KOGYO K.K., Isehara Technical Center, Isehara, Kanagawa 259-1146, Japan;* orcid.org/0000-0002-7552-3645

Donghyun Kim − *School of Electrical and Electronic Engineering, Yonsei University, Seoul 03722, Republic of Korea;* orcid.org/0000-0002-8092-6852

Yusuke Oshima − *Chemical Materials Development Department, TANAKA KIKINZOKU KOGYO K.K., Tsukuba Technical Center, Tsukuba, Ibaraki 300-4247, Japan*

Hiroki Sato − *Chemical Materials Development Department, TANAKA KIKINZOKU KOGYO K.K., Tsukuba Technical Center, Tsukuba, Ibaraki 300-4247, Japan*

Complete contact information is available at: https://pubs.acs.org/10.1021/acsomega.1c03463

Notes

The authors declare no competing financial interest.

■ ACKNOWLEDGMENTS

This work was supported by TANAKA KIKINZOKU KOGYO K.K.

■ REFERENCES

(1) Subramanian, V.; Chang, J. B.; De La Fuente Vornbrock, A.; Huang, D. C.; Jagannathan, L.; Liao, F.; Mattis, B.; Molesa, S.; Redinger, D. R.; Soltman, D.; Volkman, S. K.; Zhang, Q. In *Printed Electronics for Low-Cost Electronic Systems: Technology Status and Application Development*, ESSCIRC 2008-34th European Solid-State Circuits Conference; IEEE, 2008; pp 17−24.

(2) Kwon, J. H.; Pode, R.; Kim, H. D.; Chung, H. K. High-Performance Organic Light-Emitting Diode Displays. In *Applications of Organic and Printed Electronics*; Springer: Boston, MA, 2013; pp 57−81. https://doi.org/10.1007/978-1-4614-3160-2_3.

(3) Chou, K.-S.; Huang, K.-C.; Lee, H.-H. Fabrication and Sintering Effect on the Morphologies and Conductivity of Nano-Ag Particle Films by the Spin Coating Method. *Nanotechnology* **2005**, *16*, 779−784.

(4) Buffat, P.; Borel, J. P. Size Effect on the Melting Temperature of Gold Particles. *Phys. Rev. A* **1976**, *13*, 2287−2298.

(5) Dearden, A. L.; Smith, P. J.; Shin, D. Y.; Reis, N.; Derby, B.; O'Brien, P. A Low Curing Temperature Silver Ink for Use in Ink-Jet Printing and Subsequent Production of Conductive Tracks. *Macromol. Rapid Commun.* **2005**, *26*, 315−318.

(6) Yoon, S.; Kim, H. K. Cost-Effective Stretchable Ag Nanoparticles Electrodes Fabrication by Screen Printing for Wearable Strain Sensors. *Surf. Coat. Technol.* **2020**, *384*, No. 125308.

(7) Yamada, T.; Fukuhara, K.; Matsuoka, K.; Minemawari, H.; Tsutsumi, J.; Fukuda, N.; Aoshima, K.; Arai, S.; Makita, Y.; Kubo, H.; Enomoto, T.; Togashi, T.; Kurihara, M.; Hasegawa, T. Nanoparticle Chemisorption Printing Technique for Conductive Silver Patterning with Submicron Resolution. *Nat. Commun.* **2016**, *7*, No. 11402.

(8) Trotter, M.; Juric, D.; Bagherian, Z.; Borst, N.; Gläser, K.; Meissner, T.; Stetten, F.; von Zimmermann, A. Inkjet-Printing of Nanoparticle Gold and Silver Ink on Cyclic Olefin Copolymer for DNA-Sensing Applications. *Sensors* **2020**, *20*, No. 1333.

(9) Bernechea, M.; Miller, N. C.; Xercavins, G.; So, D.; Stavrinadis, A.; Konstantatos, G. Solution-Processed Solar Cells Based on

Environmentally Friendly $AgBiS_2$ Nanocrystals. *Nat. Photonics* **2016**, *10*, 521−525.
(10) Seker, F.; Meeker, K.; Kuech, T. F.; Ellis, A. B. Surface Chemistry of Prototypical Bulk II-VI and III-V Semiconductors and Implications for Chemical Sensing. *Chem. Rev.* **2000**, *100*, 2505−2536.
(11) Smith, A. M.; Duan, H.; Rhyner, M. N.; Ruan, G.; Nie, S. A Systematic Examination of Surface Coatings on the Optical and Chemical Properties of Semiconductor Quantum Dots. *Phys. Chem. Chem. Phys.* **2006**, *8*, 3895−3903.
(12) Do, S.; Kwon, W.; Rhee, S. W. Soft-Template Synthesis of Nitrogen-Doped Carbon Nanodots: Tunable Visible-Light Photoluminescence and Phosphor-Based Light-Emitting Diodes. *J. Mater. Chem. C* **2014**, *2*, 4221−4226.
(13) Kumar, Y.; Kumar, H.; Rawat, G.; Kumar, C.; Sharma, A.; Pal, B. N.; Jit, S. Colloidal ZnO Quantum Dots Based Spectrum Selective Ultraviolet Photodetectors. *IEEE Photonics Technol. Lett.* **2017**, *29*, 361−364.
(14) Reda, S. M. Synthesis and Optical Properties of CdS Quantum Dots Embedded in Silica Matrix Thin Films and Their Applications as Luminescent Solar Concentrators. *Acta Mater.* **2008**, *56*, 259−264.
(15) Yu, H.; Wang, H.; Zhang, J.; Lu, J.; Yuan, Z.; Xu, W.; Hultman, L.; Bakulin, A. A.; Friend, R. H.; Wang, J.; Liu, X. K.; Gao, F. Efficient and Tunable Electroluminescence from In Situ Synthesized Perovskite Quantum Dots. *Small* **2019**, *15*, No. 1804947.
(16) Zeng, P.; Zajac, S.; Clapp, P. C.; Rifkin, J. A. Nanoparticle Sintering Simulations. *Mater. Sci. Eng., A* **1998**, *252*, 301−306.
(17) Turyanska, L.; Elfurawi, U.; Li, M.; Fay, M. W.; Thomas, N. R.; Mann, S.; Blokland, J. H.; Christianen, P. C. M.; Patanè, A. Tailoring the Physical Properties of Thiol-Capped PbS Quantum Dots by Thermal Annealing. *Nanotechnology* **2009**, *20*, No. 315604.
(18) Gao, J.; Zhang, J.; Van De Lagemaat, J.; Johnson, J. C.; Beard, M. C. Charge Generation in PbS Quantum Dot Solar Cells Characterized by Temperature-Dependent Steady-State Photoluminescence. *ACS Nano* **2014**, *8*, 12814−12825.
(19) Yao, X.; Liu, S.; Chang, Y.; Li, G.; Mi, L.; Wang, X.; Jiang, Y. PbS Quantum-Dot Depleted Heterojunction Solar Cells Employing CdS Nanorod Arrays as the Electron Acceptor with Enhanced Efficiency. *ACS Appl. Mater. Interfaces* **2015**, *7*, 23117−23123.
(20) Van Embden, J.; Della Gaspera, E. Ultrathin Solar Absorber Layers of Silver Bismuth Sulfide from Molecular Precursors. *ACS Appl. Mater. Interfaces* **2019**, *11*, 16674−16682.
(21) European Commission Waste Electrical & Electronic Equipment. Directive 2011/65/EU of the European Parliament and of the Council of 8 June 2011 on the Restriction of the Use of Certain Hazardous Substances in Electrical and Electronic Equipment Text with EEA Relevance. *Off. J. Eur. Union* **2011**, *1*, 88−110.
(22) Rogalski, A. Infrared Detectors: An Overview. *Infrared Phys. Technol.* **2002**, *43*, 187−210.
(23) Guin, S. N.; Biswas, K. Cation Disorder and Bond Anharmonicity Optimize the Thermoelectric Properties in Kinetically Stabilized Rocksalt AgBiS2 Nanocrystals. *Chem. Mater.* **2013**, *25*, 3225−3231.
(24) Zamiri, R.; Ahangar, H. A.; Zakaria, A.; Zamiri, G.; Shabani, M.; Singh, B.; Ferreira, J. M. F. The Structural and Optical Constants of Ag_2S Semiconductor Nanostructure in the Far-Infrared. *Chem. Cent. J.* **2015**, *9*, No. 28.
(25) Akamatsu, K.; Takei, S.; Mizuhata, M.; Kajinami, A.; Deki, S.; Takeoka, S.; Fujii, M.; Hayashi, S.; Yamamoto, K. Preparation and Characterization of Polymer Thin Films Containing Silver and Silver Sulfide Nanoparticles. *Thin Solid Films* **2000**, *359*, 55−60.
(26) Pejova, B.; Nesheva, D.; Aneva, Z.; Petrova, A. Photoconductivity and Relaxation Dynamics in Sonochemically Synthesized Assemblies of $AgBiS_2$ Quantum Dots. *J. Phys. Chem. C* **2011**, *115*, 37−46.
(27) Yang, W.; Xie, T.; Jiang, T.; Wang, D. Facile Preparation of Ag_2S Nanoparticles with Broad Photoelectric Response Region. *Colloids Surf., A* **2013**, *433*, 55−58.
(28) Pejova, B.; Grozdanov, I.; Nesheva, D.; Petrova, A. Size-Dependent Properties of Sonochemically Synthesized Three-Dimensional Arrays of Close-Packed Semiconducting AgBiS2 Quantum Dots. *Chem. Mater.* **2008**, *20*, 2551−2565.
(29) Huang, P.; Yang, W.; Lee, M. AgBiS2 Semiconductor-Sensitized Solar Cells. *Journal of Physical Chemistry C* **2013**, *117*, 18308−18314.
(30) Hu, L.; Patterson, R. J.; Zhang, Z.; Hu, Y.; Li, D.; Chen, Z.; Yuan, L.; Teh, Z. L.; Gao, Y.; Conibeer, G. J.; Huang, S. Enhanced Optoelectronic Performance in $AgBiS_2$ Nanocrystals Obtained via an Improved Amine-Based Synthesis Route. *J. Mater. Chem. C* **2018**, *6*, 731−737.
(31) Liang, N.; Chen, W.; Dai, F.; Wu, X.; Zhang, W.; Li, Z.; Shen, J.; Huang, S.; He, Q.; Zai, J.; Fang, N.; Qian, X. Homogenously Hexagonal Prismatic $AgBiS_2$ Nanocrystals: Controlled Synthesis and Application in Quantum Dot-Sensitized Solar Cells. *CrystEngComm* **2015**, *17*, 1902−1905.
(32) Zhong, J.; Xiang, W.; Xie, C.; Liang, X.; Xu, X. Synthesis of Spheroidal $AgBiS_2$ Microcrystals by L-Cysteine Assisted Method. *Mater. Chem. Phys.* **2013**, *138*, 773−779.
(33) Kang, M. H.; Kim, S. H.; Jang, S.; Lim, J. E.; Chang, H.; Kong, K. J.; Myung, S.; Park, J. K. Synthesis of Silver Sulfide Nanoparticles and Their Photodetector Applications. *RSC Adv.* **2018**, *8*, 28447−28452.
(34) Chukwuocha, E. O.; Onyeaju, M. C.; Harry, T. S. T. Theoretical Studies on the Effect of Confinement on Quantum Dots Using the Brus Equation. *World J. Condens. Matter Phys.* **2012**, *2*, 96−100.
(35) Pan, J.; Quan, L. N.; Zhao, Y.; Peng, W.; Murali, B.; Sarmah, S. P.; Yuan, M.; Sinatra, L.; Alyami, N. M.; Liu, J.; Yassitepe, E.; Yang, Z.; Voznyy, O.; Comin, R.; Hedhili, M. N.; Mohammed, O. F.; Lu, Z. H.; Kim, D. H.; Sargent, E. H.; Bakr, O. M. Highly Efficient Perovskite-Quantum-Dot Light-Emitting Diodes by Surface Engineering. *Adv. Mater.* **2016**, *28*, 8718−8725.
(36) Protesescu, L.; Yakunin, S.; Bodnarchuk, M. I.; Krieg, F.; Caputo, R.; Hendon, C. H.; Yang, R. X.; Walsh, A.; Kovalenko, M. V. Nanocrystals of Cesium Lead Halide Perovskites ($CsPbX_3$, X = Cl, Br, and I): Novel Optoelectronic Materials Showing Bright Emission with Wide Color Gamut. *Nano Lett.* **2015**, *15*, 3692−3696.
(37) Song, J.; Li, J.; Xu, L.; Li, J.; Zhang, F.; Han, B.; Shan, Q.; Zeng, H. Room-Temperature Triple-Ligand Surface Engineering Synergistically Boosts Ink Stability, Recombination Dynamics, and Charge Injection toward EQE-11.6% Perovskite QLEDs. *Adv. Mater.* **2018**, *30*, No. 1800764.
(38) Kim, D.; Kim, D. H.; Lee, J. H.; Grossman, J. C. Impact of Stoichiometry on the Electronic Structure of PbS Quantum Dots. *Phys. Rev. Lett.* **2013**, *110*, No. 196802.
(39) Santos, F. J. V.; Nieto De Castro, C. A.; Dymond, J. H.; Dalaouti, N. K.; Assael, M. J.; Nagashima, A. Standard Reference Data for the Viscosity of Toluene. *J. Phys. Chem. Ref. Data* **2006**, *35*, No. 1928233.
(40) Wang, S.; Gao, Q.; Wang, J. Thermodynamic Analysis of Decomposition of Thiourea and Thiourea Oxides. *J. Phys. Chem. B* **2005**, *109*, 17281−17289.
(41) Sharma, R. C.; Chang, Y. A. The Ag-S (Silver-Sulfur) System. *Bull. Alloy Phase Diagrams* **1986**, *7*, 263−269.
(42) Voronin, M. V.; Osadchii, E. G. Determination of Thermodynamic Properties of Triple Phases Formed in Different Regions of Phase Diagram of the Ag-Bi-S System Using EMF Measurements. *Russ. J. Electrochem.* **2013**, *49*, 741−746.
(43) Moulder, J. F.; Stickle, W. F.; Sobol, P. E.; Bomben, K. D. *Handbook of X-Ray Photoelectron Spectroscopy*; Chastain, J., Ed.; Perkin-Elmer Corporation Physical Electronics Division: Minnesota, USA, 1992. https://doi.org/10.1002/0470014229.ch22.
(44) Wilson, D.; Langell, M. A. XPS Analysis of Oleylamine/Oleic Acid Capped Fe_3O_4 Nanoparticles as a Function of Temperature. *Appl. Surf. Sci.* **2014**, *303*, 6−13.

https://doi.org/10.1021/acsomega.1c03463
ACS Omega 2021, 6, 20710−20718

(45) Criddle, W. J.; Thomas, J. Pyrolysis—Gas Chromatography of Quaternary Ammonium Salts in Aqueous Solution. *J. Anal. Appl. Pyrolysis* **1961**, *2*, 361−366.
(46) VonNiederhausern, D. M.; Wilson, G. M.; Giles, N. F. Critical Point and Vapor Pressure Measurements for Seven Compounds by a Low Residence Time Flow Method. *J. Chem. Eng. Data* **2006**, *51*, 1982−1985.
(47) Theo Kloprogge, J.; Wood, B. J. *Handbook of Mineral Spectroscopy*; Elsevier, 2021; Vol. *1*. https://doi.org/10.1016/b978-0-12-804522-0.01001-4.
(48) Han, S. W.; Kim, Y.; Kim, K. Dodecanethiol-Derivatized Au/Ag Bimetallic Nanoparticles: TEM, UV/VIS, XPS, and FTIR Analysis. *J. Colloid Interface Sci.* **1998**, *208*, 272−278.
(49) West, W. A.; Menzies, A. W. C. The Vapor Pressures of Sulfur between 100° and 550° with Related Thermal Data. *J. Phys. Chem. A* **1929**, *33*, 1880−1892.
(50) Lee, D. H.; Condrate, R. A.; Lacourse, W. C. FTIR Spectral Characterization of Thin Film Coatings of Oleic Acid on Glasses: Part II Coatings on Glass from Different Media Such as Water, Alcohol, Benzene and Air. *J. Mater. Sci.* **2000**, *35*, 4961−4970.
(51) Bronstein, L. M.; Huang, X.; Retrum, J.; Schmucker, A.; Pink, M.; Stein, B. D.; Dragnea, B. Influence of Iron Oleate Complex Structure on Iron Oxide Nanoparticle Formation. *Chem. Mater.* **2007**, *19*, 3624−3632.
(52) Lee, D. H.; Condrate, R. A. FTIR Spectral Characterization of Thin Film Coatings of Oleic Acid on Glasses: I. Coatings on Glasses from Ethyl Alcohol. *J. Mater. Sci.* **1999**, *34*, 139−146.
(53) Erley, W.; Hemminger, J. C. Spectroscopic Identification of an HCNH Species on Pt(111). *Surf. Sci.* **1994**, *316*, L1025−L1030.
(54) Wang, H.; Jiao, X.; Chen, D. Monodispersed Nickel Nanoparticles with Tunable Phase and Size: Synthesis, Characterization, and Magnetic Properties. *J. Phys. Chem. C* **2008**, *112*, 18793−18797.
(55) Salavati-Niasari, M.; Fereshteh, Z.; Davar, F. Synthesis of Oleylamine Capped Copper Nanocrystals via Thermal Reduction of a New Precursor. *Polyhedron* **2009**, *28*, 126−130.
(56) Xu, F.; Gerlein, L. F.; Ma, X.; Haughn, C. R.; Doty, M. F.; Cloutier, S. G. Impact of Different Surface Ligands on the Optical Properties of PbS Quantum Dot Solids. *Materials* **2015**, *8*, 1858−1870.
(57) Sadovnikov, S. I.; Vovkotrub, E. G. Thermal Stability of Nanoparticle Size and Phase Composition of Nanostructured Ag_2S Silver Sulfide. *J. Alloys Compd.* **2018**, *766*, 140−148.
(58) Liu, P. S.; Chen, G. F. *Porous Materials: Processing and Applications*; Butterworth-Heinemann, 2014. https://doi.org/10.1016/C2012-0-03669-1.
(59) Craig, J. R. Phase Relations and Mineral Assemblages in the Ag-Bi-Pb-S System. *Miner. Deposits* **1967**, *1*, 278−306.
(60) Vaitkus, A.; Merkys, A.; Gražulis, S. Validation of the Crystallography Open Database Using the Crystallographic Information Framework. *J. Appl. Crystallogr.* **2021**, *54*, 661−672.
(61) Quirós, M.; Gražulis, S.; Girdzijauskaitė, S.; Merkys, A.; Vaitkus, A. Using SMILES Strings for the Description of Chemical Connectivity in the Crystallography Open Database. *J. Cheminf.* **2018**, *10*, 1−17.
(62) Merkys, A.; Vaitkus, A.; Butkus, J.; Okulič-Kazarinas, M.; Kairys, V.; Gražulis, S. COD::CIF::Parser: An Error-Correcting CIF Parser for the Perl Language. *J. Appl. Crystallogr.* **2016**, *49*, 292−301.
(63) Gražulis, S.; Merkys, A.; Vaitkus, A.; Okulič-Kazarinas, M. Computing Stoichiometric Molecular Composition from Crystal Structures. *J. Appl. Crystallogr.* **2015**, *48*, 85−91.
(64) Gražulis, S.; Daškevič, A.; Merkys, A.; Chateigner, D.; Lutterotti, L.; Quirós, M.; Serebryanaya, N. R.; Moeck, P.; Downs, R. T.; Le Bail, A. Crystallography Open Database (COD): An Open-Access Collection of Crystal Structures and Platform for World-Wide Collaboration. *Nucleic Acids Res.* **2012**, *40*, 420−427.
(65) Graulis, S.; Chateigner, D.; Downs, R. T.; Yokochi, A. F. T.; Quirós, M.; Lutterotti, L.; Manakova, E.; Butkus, J.; Moeck, P.; Le Bail, A. Crystallography Open Database - An Open-Access Collection of Crystal Structures. *J. Appl. Crystallogr.* **2009**, *42*, 726−729.
(66) Downs, R. T.; Hall-Wallace, M. The American Mineralogist Crystal Structure Database. *Am. Mineral.* **2003**, *88*, 247−250.
(67) Altomare, A.; Cuocci, C.; Giacovazzo, C.; Moliterni, A.; Rizzi, R. QUALX: A Computer Program for Qualitative Analysis Using Powder Diffraction Data. *J. Appl. Crystallogr.* **2008**, *41*, 815−817.
(68) Altomare, A.; Corriero, N.; Cuocci, C.; Falcicchio, A.; Moliterni, A.; Rizzi, R. QUALX2.0: A Qualitative Phase Analysis Software Using the Freely Available Database POW-COD. *J. Appl. Crystallogr.* **2015**, *48*, 598−603.
(69) Hwang, B. H. Calculation and Measurement of All (002) Multiple Diffraction Peaks from a (001) Silicon Wafer. *J. Phys. D: Appl. Phys.* **2001**, *34*, 2469−2474.
(70) Geller, S.; Wernick, J. H. Ternary Semiconducting Compounds with Sodium Chloride-like Structure: $AgSbSe_2$, $AgSbTe_2$, $AgBiS_2$, $AgBiSe_2$. *Acta Crystallogr.* **1959**, *12*, 46−54.
(71) Wuensch, B. J.; Cava, R. J.; Reidinger, F. Single-Crystal Neutron Diffraction Study of the Fast-Ion Conductor β-Ag_2S between 186 and 325 °C. *J. Solid State Chem.* **1980**, *31*, 69−80.
(72) Makovicky, E.; Mumme, W. G.; Watts, J. A. The Crystal Structure of Synthetic Pavonite, $AgBi_3S_5$, and the Definition of the Pavonite Homologous Series. *Can. Mineral.* **1977**, *15*, 339−348.
(73) Spreadborough, J.; Christian, J. W. High-Temperature X-Ray Diffractometer. *J. Sci. Instrum.* **1959**, *36*, 116−118.
(74) Uematsu, T.; Wajima, K.; Sharma, D. K.; Hirata, S.; Yamamoto, T.; Kameyama, T.; Vacha, M.; Torimoto, T.; Kuwabata, S. Narrow Band-Edge Photoluminescence from AgInS2 Semiconductor Nanoparticles by the Formation of Amorphous III−VI Semiconductor Shells. *NPG Asia Mater.* **2018**, *10*, 713−726.
(75) ImageJ. https://imagej.nih.gov/ij/ (accessed May 5, 2021).
(76) Schneider, C. A.; Rasband, W. S.; Eliceiri, K. W. NIH Image to ImageJ: 25 Years of Image Analysis. *Nat. Methods* **2012**, *9*, 671−675.
(77) Abràmoff, M. D.; Magalhães, P. J.; Ram, S. J. Image Processing with ImageJ. *Biophotonics Int.* **2004**, *11*, 36−41.

https://doi.org/10.1021/acsomega.1c03463
ACS Omega 2021, 6, 20710−20718